

## The Synthesis of LiFePO<sub>4</sub>/C Composite by the Precipitation Between Two Water/Oil Emulsions

Sih-Ci Jheng, Jenn-Shing Chen\*

Department of Applied Chemistry, National University of Kaohsiung, Kaohsiung City, Taiwan 811, R.O.C.

\*E-mail: [jschen@nuk.edu.tw](mailto:jschen@nuk.edu.tw)

Received: 12 February 2013 / Accepted: 28 February 2013 / Published: 1 April 2013

---

Microparticles of LiFePO<sub>4</sub>/C composites are prepared as cathode materials for lithium rechargeable batteries by precipitation between two emulsion solutions. The aqueous cores of the microemulsions are used as constrained microreactors for the precipitation of the precursors for the nano-composite. Calcination at 600°C results in microcrystalline LiFePO<sub>4</sub>/C composite powders. Using this method, well-crystallized LiFePO<sub>4</sub>/C with an olivine type structure is synthesized. The materials are characterized by X-ray diffraction (XRD), scanning electron microscopy (SEM), transmission electron microscopy (TEM), particle size analysis (PSA), BET surface area, cyclic voltammetry (CV), electrochemical impedance spectroscopy (EIS) and charge-discharge tests. The electrochemical performance of micro-sized LiFePO<sub>4</sub>-C composites is improved compared to composites obtained by classical co-precipitation methods. The composites exhibit a noticeably improved performance at high rates, with higher initial capacity values and a good cycle life.

---

**Keywords:** LiFePO<sub>4</sub>, Microemulsion, Lithium ion battery

### 1. INTRODUCTION

Olivine LiFePO<sub>4</sub> has been widely studied and is a good candidate for a cathode material for Li-ion batteries, because of its high theoretical capacity (170 mAh/g), cycling stability, low cost and environmental friendliness. These attractive characteristics make olivine LiFePO<sub>4</sub> highly suitable for use in large-scale Li-ion batteries for electric vehicles (EV) and hybrid electric vehicles (HEV) applications. Despite these favorable characteristics, their widespread use is hampered by its poor rate performance. The salient feature responsible for its poor rate capability is thought to be its intrinsically poor electronic conductivity (of the order of 10<sup>-9</sup> S cm<sup>-1</sup>) and the sluggish Li<sup>+</sup> diffusion that occurs across the LiFePO<sub>4</sub>/FePO<sub>4</sub> interface [1-3].

In order to overcome these problems, several strategies have been used over the years, from optimized synthesis procedures [4,5], carbon nanocoating [6,7], particle-size minimization [8] and metal powder addition [9,10], to doping with alien cations [11] or the carbothermal formation of the surface conducting phase [11-14]. To date, the majority of these studies have focused on the incorporation of conductive carbon into active material powders to form carbon-coated  $\text{LiFePO}_4$  ( $\text{LiFePO}_4/\text{C}$ ) composites. The behavior of these  $\text{LiFePO}_4/\text{C}$  composites is related to the phase purity of the active material, particle size, structure of the carbon additive, the carbon content, form of carbon contact, and the mixing and sintering recipe.

The reverse emulsion technique is a well-know method and was successfully applied to many ceramic systems to prepare microsized ceramic particles with spherical morphology and narrow size distribution, e.g.  $\text{Y}_2\text{O}_3$ ,  $\text{Al}_2\text{O}_3$ ,  $\text{TiO}_2$  and  $\text{ZrO}_2$  [15 –17]. In the reverse emulsion, a surfactant was added into the mixture of the oil and water to lower the interfacial tension between the oil/water phases. When an appropriate value of hydrophile-lipophile-balance (HLB) was used, a water-in-oil emulsion was obtained [18]. In this work, a two reverse-emulsion technique was adopted to prepare electroactive carbon-coated  $\text{LiFePO}_4$  particles. The aqueous cores formed by contact between two reverse-emulsion solutions were used as highly constrained microreactors for the precipitation of nano-amorphous  $\text{LiFePO}_4$ . Figure 1 displays a schematic illustration of the precipitation method between two reverse-emulsion solutions.

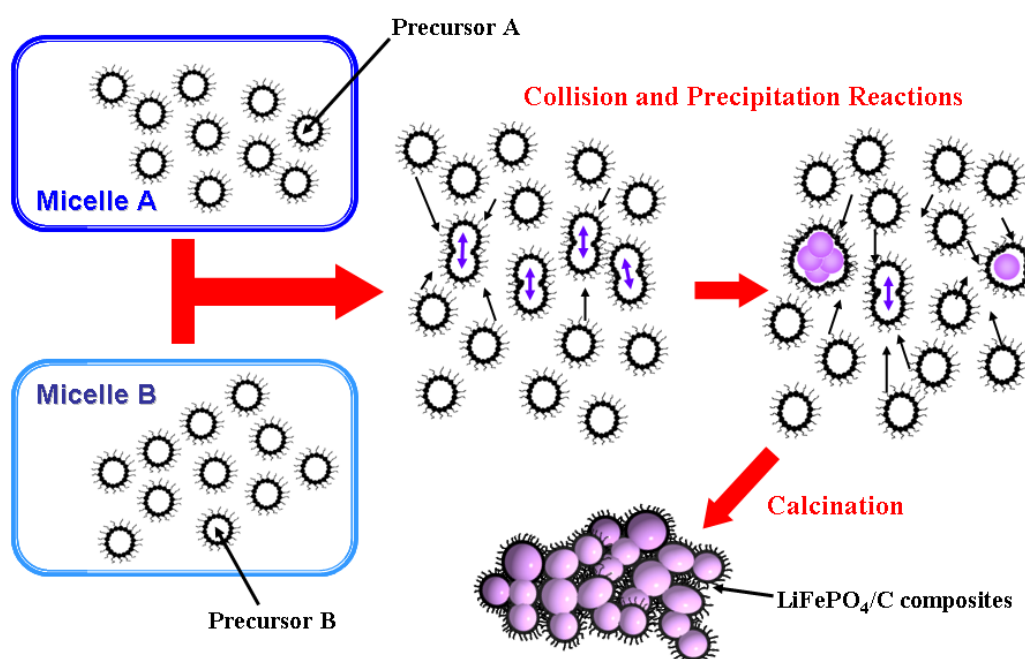


**Figure 1.** Schematic illustration of the precipitation method between two reverse-emulsion solutions.

Recently, the relationship of the performance of  $\text{LiFePO}_4/\text{C}$  composites to the carbon structural parameters derived from Raman analysis has been investigated [12-14]. These results indicate that the carbon precursors chosen directly affected the characteristics of the carbon additive, which in turn are

related to the performance of the  $\text{LiFePO}_4/\text{C}$  composite. The selection of organic precursors as a carbon source is very important for tailoring the final properties of carbon coated composite powders. According to our earlier studies [19-22], the choice of an appropriate organic precursor as a carbon source is suitable to produce a  $\text{LiFePO}_4/\text{C}$  composite with a fine particle size and a uniformly coated carbon conductive layer, which exhibited better electrochemical performance. In this work, we used several nonionic organic compounds as surfactants to produce the aqueous cores in the microemulsion. The surfactants formed residual carbon on the surface of the  $\text{LiFePO}_4$  particles after calcinating the cores, as shown in Fig.1. The nonionic organic surfactants, Brij-30 (Polyethylene glycol dodecyl ether), Igepal-520 (Polyethylene(5) nonylphenyl ether) and PPGBE (Poly(propylene glycol) monobutyl ether) were used as carbon precursors to study their influence on the behavior of the  $\text{LiFePO}_4/\text{C}$  composite. The physicochemical properties and electrochemical behavior of the samples were characterized.

## 2. EXPERIMENTAL

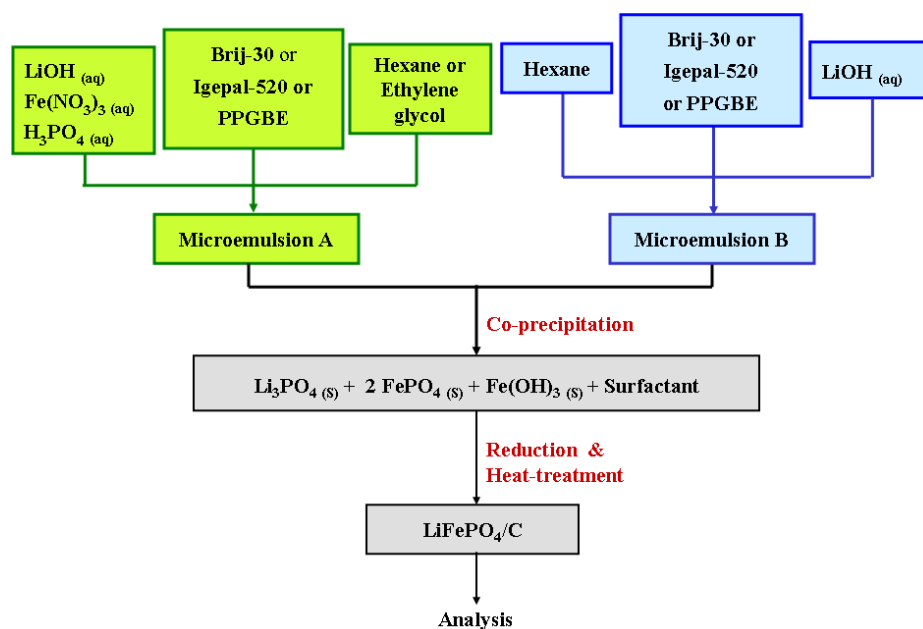


**Figure 2.** Flowchart for preparing  $\text{LiFePO}_4/\text{C}$  powder by the precipitation method between two microemulsion solutions.

The flow chart for the preparing  $\text{LiFePO}_4$  and its carbon composites in the two reverse-emulsions was shown in Fig.2. The first step was to prepare two microemulsion A and B solutions, respectively. Microemulsion A was prepared by dissolving  $\text{LiOH} \cdot \text{H}_2\text{O}$  (TEDIA),  $\text{Fe}(\text{NO}_3)_3 \cdot 9\text{H}_2\text{O}$  (Riedel-deHaen) and  $\text{H}_3\text{PO}_4$  (J.T. Baker) in 5ml de-ioned water at 1:1:1 Li:Fe:P molar ratio, which was vigorously mixed with a mixtures of an oily phase for 6.5g Brij-30 (Sigma-Aldrich) or 10g Igepal-520 (Sigma-Aldrich) in 50ml hexane (J.T. Baker) or 50g PPGBE (Sigma-Aldrich) in 10g ethylene glycol (J.T. Baker). Microemulsion B was mixed 5 ml  $0.68 \text{ mol l}^{-1}$   $\text{LiOH} \cdot \text{H}_2\text{O}$  and 5g Brij-30 or 11.25g

Igepal-520 in 50ml hexane or 50g PPGBE in 10g ethylene glycol. The two stable emulsions of micelle A and B were mixed and stirred with a magnetic stirrer under room temperature for 30 min to form gelled  $\text{LiFePO}_4$  precursor particles. The precipitates of  $\text{LiFePO}_4$  precursor particles were collected by an ultracentrifuge and then heated at  $120^\circ\text{C}$  to evaporate water and organic solvents. After drying, the precursor powders were ground and heat-treated in a tubular furnace at  $600^\circ\text{C}$  for 12 h under reducing atmosphere ( $\text{Ar}/\text{H}_2 = 95/5$ ) to yield  $\text{LiFePO}_4/\text{C}$  composite materials.

A Rigaku-D/MaX-2550 diffractometer with  $\text{Cu K}\alpha$  radiation ( $\lambda=1.54 \text{ \AA}$ ) was used to obtain X-ray diffraction (XRD) patterns for the samples. The morphology of the sample was observed by a scanning electron microscope (SEM, Hitachi S-4300) and transmission electron microscope (TEM, JEOL JEM-2010). Particle size analysis (PSA) was carried out with a Malvern particle size analyzer (Zetasizer Nano ZS). The Brunauer-Emmett-Teller (BET) method was used to measure the specific surface area of powders (ASAP2020). The residual carbon content of the powders was determined by means of an automatic elemental analyzer (EA, Elementar vario, EL III).

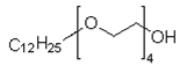
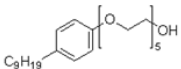
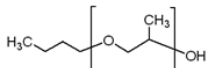
For electrochemical evaluation, the composite electrodes were prepared by wet coating, and were made from as-prepared  $\text{LiFePO}_4/\text{C}$  with acetylene black, SFG-6 synthetic flake graphite (Timcal Ltd.), and poly(vinylidene difluoride) (PVdF) binder (MKB-212C, Elf Atochem) in a weight ratio of 80:5:5:10. The  $\text{LiFePO}_4/\text{C}$  active materials, acetylene black and SFG-6 were first added to a solution of PVdF in N-methyl-2-pyrrolidone (NMP, Riedel-deHaen). The mixture was stirred for 20 minutes at room temperature with a magnetic bar, and then with a turbine for 5 minutes at 2000 rpm to make a slurry with an appropriate viscosity. The resulting slurry was coated onto a piece of aluminum foil and dried at  $120^\circ\text{C}$  for 40 min. The coating had a thickness of  $\sim 100 \mu\text{m}$  with an active material mass loading of  $8 \pm 1 \text{ mg cm}^{-2}$ . The quantity of active materials on the electrodes was kept constant. Electrodes were dried overnight at  $100^\circ\text{C}$  under vacuum before being transferred to an argon-filled glove box for cell assembly. Electrodes were placed in an open glass bottle cell with a  $1 \text{ cm}^2$  square  $\text{LiFePO}_4/\text{C}$  cathode electrode and lithium foil as the counter and reference electrodes for CV experiment. Coin cells of 2032 size were assembled using lithium metal as a counter electrode. A solution of 1 M  $\text{LiPF}_6$  in a mixed solvent of ethylene carbonate/dimethyl carbonate (EC/DMC) with 1:1 volume ratio was used as the electrolyte in all cells. The CV and EIS experiments were carried out with a CHI 704A potentiostat at a scan rate of  $0.1 \text{ mV s}^{-1}$  for CV test. During EIS measurement, the excitation voltage applied to the cells was 5 mV and the frequency range was between 100 kHz and 10 mHz. Coin cells were cycled galvanostatically with a BAT-750B (Acu Tech System) at a constant current of 0.1C with a voltage region of 2.5–4.2 V vs  $\text{Li}/\text{Li}^+$  at room temperature; here, 1C equals 170  $\text{mA g}^{-1}$ . The specific capacity was calculated based on the mass of active material in the electrode.

### 3. RESULTS AND DISCUSSION

According to previous reports [23-24], the preparation of a carbon-coated  $\text{LiFePO}_4$  ( $\text{LiFePO}_4/\text{C}$ ) with a smaller particle size would be preferred to improve the capacity and the limited rate capability of  $\text{LiFePO}_4$ . For these reasons, a precipitation method between two reverse-emulsions was employed to prepare a smaller particle size of  $\text{LiFePO}_4/\text{C}$  composite in this study. During the

synthesis of  $\text{LiFePO}_4/\text{C}$  composites by the emulsion-precipitation method, the final quality of  $\text{LiFePO}_4/\text{C}$  powder was affected by many factors such as type and concentration of surfactant, salt concentration, HLB value and mixing intensity and time of emulsion formation. Among the factors investigated in this work the most important one is the type of surfactant. There are several criteria to choose optimized surfactants that (i) are nonionic organic compounds without any metal ions and ester function groups (ii) undergo decomposition rather than evaporation during the firing process, (iii) have lower molecular weight. Therefore, in this work, three distinct types of nonionic organic reagents, Brij-30, Igepal-520 and PPGBE were studied to assess their effects as surfactants. The structures of surfactant compounds and their number average molecular weights ( $M_n$ ) are listed in Table 1.

**Table 1.** EA, DLS, BET surface area analysis for samples prepared from the co-precipitation method and microemulsions with various surfactants.

Sample	Residual carbon content (wt. %)	Particle sizes (nm)	BET surface area ( $\text{m}^2 \text{g}^{-1}$ )
Co-precipitation	2.1	306.7	10.2
Brij-30 ( $M_n=362$ ) 	4.2	272.7	90.7
Igepal-520 ( $M_n=441$ ) 	3.4	267.7	11.7
PPGBE ( $M_n=340$ ) 	2.2	237.8	15.5

Here, we adopted the sample prepared from the classical co-precipitation without surfactant as the control sample for comparison purposes since it has performed well according to our earlier studies [19]. All prepared  $\text{LiFePO}_4/\text{C}$  powders were deep black in color, in contrast to the gray color of pure  $\text{LiFePO}_4$  powders. Figure 3 shows the XRD patterns of the prepared samples from different surfactants. All peaks can be attributed to a pure and well-crystallized  $\text{LiFePO}_4$  phase, with an ordered olivine structure, indexed to the orthorhombic  $Pnmb$  space group. There are no peaks, but reflections were found in the diffractograms of carbon in the final product, which indicates that the carbon generated by the pyrolysis of the nonionic organic surfactants is amorphous in the final product. This is reasonable, because the content of the residual carbon for all prepared samples was approximately 2 - 4wt.%, as determined by EA. Table 1 presents the residual carbon content, particle size and BET surface area for all samples prepared from the co-precipitation method and microemulsions with various surfactants.

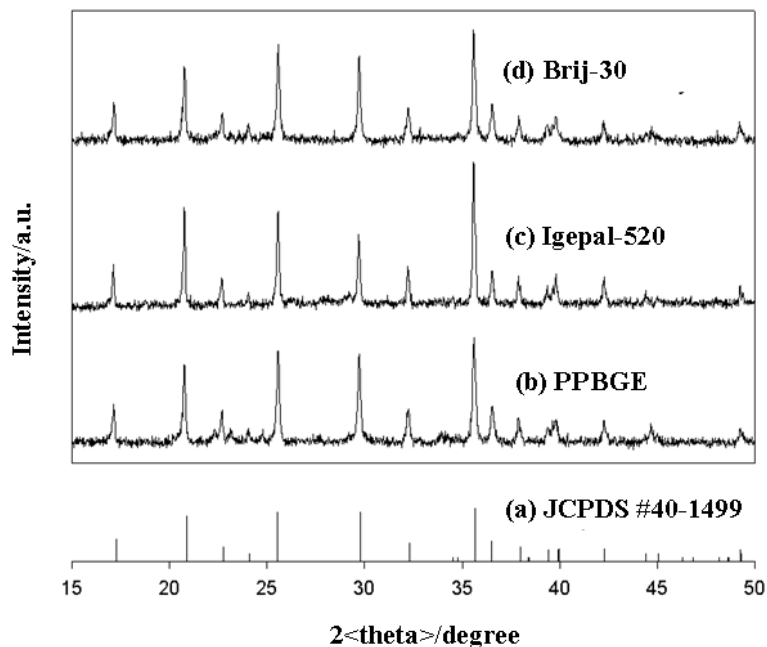


**Figure 3.** X-ray diffraction patterns of (a) theoretical  $\text{LiFePO}_4$  (JCPDS card no.40-1499)); (b) PPGBE; (c) Igepal-520; (d) Brij-30.

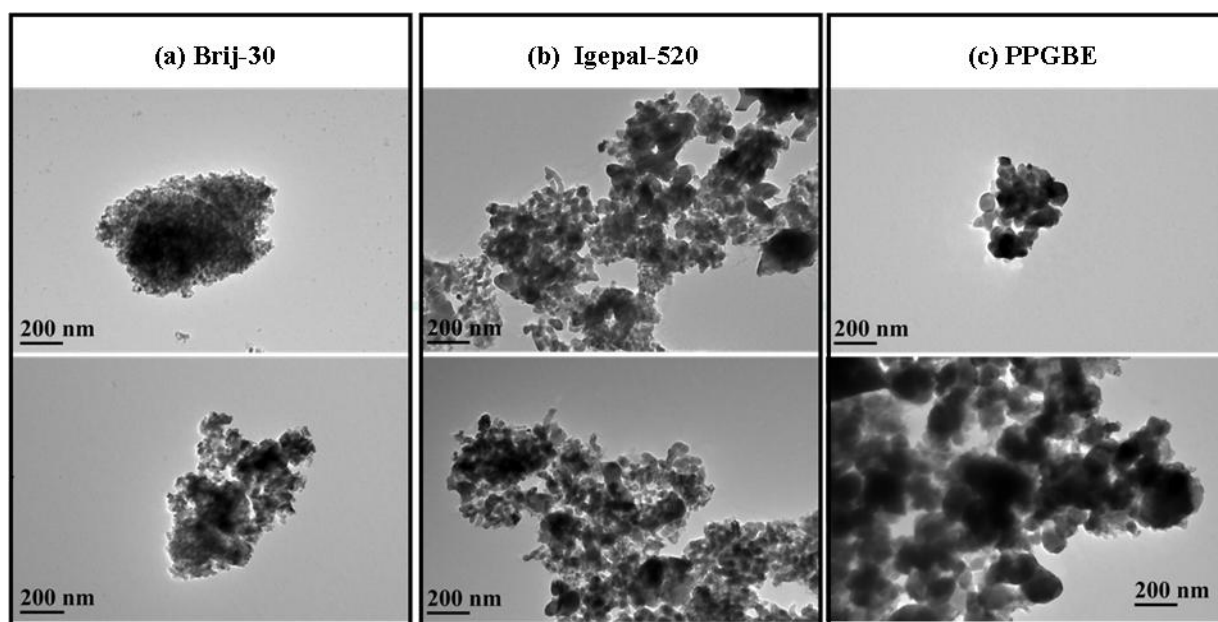
Together, this data supports that the differences in types of surfactants affect the residual carbon content, particle size and BET surface area. Dynamic light scattering (DLS) can effectively characterize the nanoparticles in solution, therefore, the dimension of resultant nanoparticles were characterized by DLS.

**Table 2.** DLS analysis of different samples prepared from the co-precipitation method and microemulsions with various surfactants.

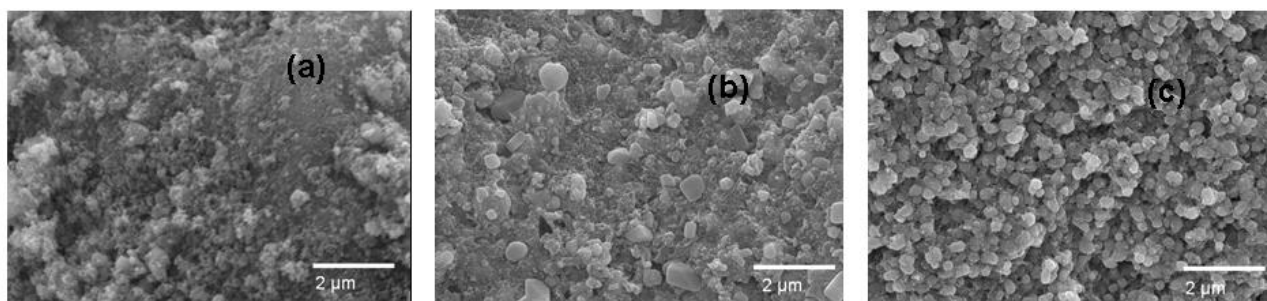
Method \ Sample	Microemulsion A	Microemulsion B	Precursor	$\text{LiFePO}_4/\text{C}$
Co-precipitation	—	—	171.1 nm and 765.1 nm	306.7 nm
Brij-30	62.02 nm	17.07 nm	137.5 nm	272.7 nm
Igepal-520	24.91 nm	26.09 nm	128.9 nm	267.7 nm
PPGBE	—	—	84.17 nm	237.8 nm

Table 2 presents the DLS analysis of different samples prepared from the co-precipitation method and with various surfactants from the microemulsions. The results exhibited that the initial aqueous cores in the microemulsion A and B have the average hydrodynamic diameters around 20 – 60 nm. The particle size of nano-amorphous  $\text{LiFePO}_4$  after the mixing of emulsion A and B is around 130nm. The small increase of particle size after the mixing can be attributed to the formation of small

aqueous cores as highly constrained microreactors for the precipitation of nano-amorphous  $\text{LiFePO}_4$  during the contact between two reverse-emulsion solutions. After calcination, the particle growth causing the formation of  $\text{LiFePO}_4/\text{C}$  composites possessing larger particle sizes. Also, Precursor particles prepared by emulsion-precipitation route were smaller than classical co-precipitation method. This can be attributed to the formation of small aqueous cores as highly constrained microreactors for the precipitation of nano-amorphous  $\text{LiFePO}_4$  during the contact between two reverse-emulsion solutions resulting in smaller particle sizes of  $\text{LiFePO}_4/\text{C}$  powders after heating the cores. Because samples prepared with Brij-30 had more carbon, its specific surface area was the most. The viscosity of PPGBE emulsion was the highest, reducing the particle collision frequency, so agglomerated particles were the smallest.



**Figure 4.** TEM images of  $\text{LiFePO}_4/\text{C}$  (a)Brij-30; (b) Igepal-520, (c) PPGBE.



**Figure 5.** SEM images of  $\text{LiFePO}_4/\text{C}$  (a)Brij-30; (b) Igepal-520, (c) PPGBE.

The TEM micrographs of  $\text{LiFePO}_4/\text{C}$  composites obtained by the pyrolysis of various surfactants are shown in Fig. 4. The relatively dark portion shown in the figure represents  $\text{LiFePO}_4$

with particle size within 200 nm, and these particles were surrounded by carbon matrix that was light gray in color. From the TEM images, it can be clearly seen that the entire carbon distribution surrounds the fine LiFePO<sub>4</sub> crystal grains like a web made of carbon. This “carbon web” leads to electronic inter-grain connection, but does not block the direct contact between the active particles and the encapsulated electrolyte. Figure 5 shows the SEM images of LiFePO<sub>4</sub>/C composites prepared from various surfactants. The general appearance of the grains in all samples is well proportioned and the size is narrowly distributed around 0.2–0.3 μm, although a few agglomerates exist. The composites appear to be framed by an amorphous carbon matrix, which contains the LiFePO<sub>4</sub> particles.

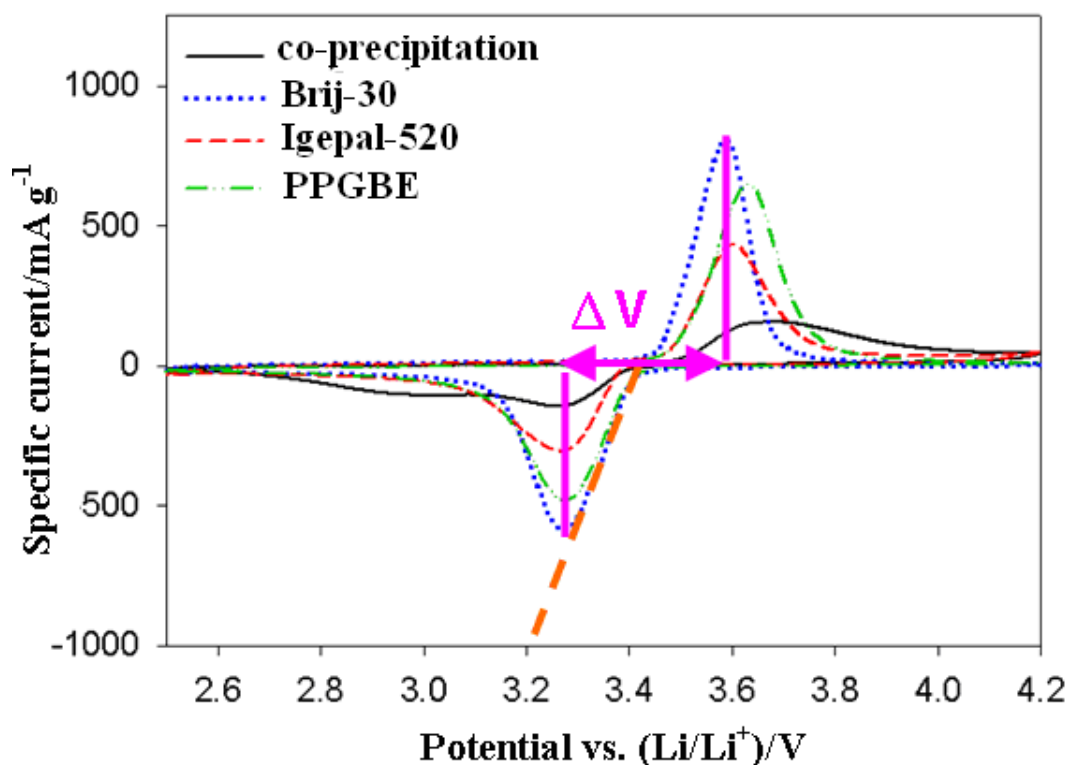


**Figure 6.** Cyclic voltammetry profile of the third cycle for LiFePO<sub>4</sub>/C prepared with various surfactants

The CV plots for different LiFePO<sub>4</sub>/C electrodes in a beaker cell, cycled between 3.0 and 4.0 V at 0.1 mV s<sup>-1</sup> and using 1M LiPF<sub>6</sub> + EC/DMC (1:1) electrolyte, are shown in Fig. 6. The CV curves of all samples exhibit two peaks, which are located at 3.6 V in the anodic sweep and 3.3 V in the cathodic sweep; these are consistent with a two-phase redox reaction at about 3.5 V vs. Li/Li<sup>+</sup>. No other peaks are present, which indicates an absence of electroactive iron impurities. The Brij-30 has a narrower peak potential separation and a larger current peak, which indicates the best reversibility of the electrode reaction and the best kinetic behavior.

Electrochemical impedance spectroscopy was measured on the coin cells in the fully charge state. Figure 7 shows the typical Nyquist plots for the spectra of all of the prepared samples. All of the spectra have an intercept at high frequency, followed by a semicircular plot in the medium-to-high

frequency region and a sloping line in the low frequency region. The intercept at the  $Z'$  axis in the high frequency region corresponds to the ohmic resistance ( $R_e$ ) of the electrolyte and the electrical contact.

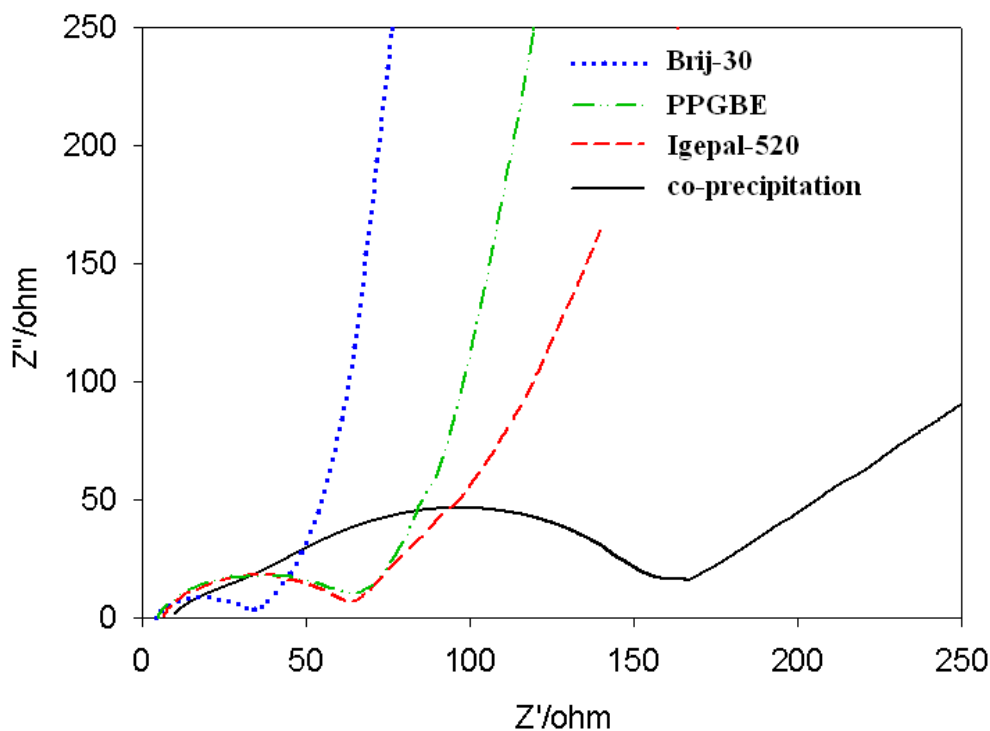
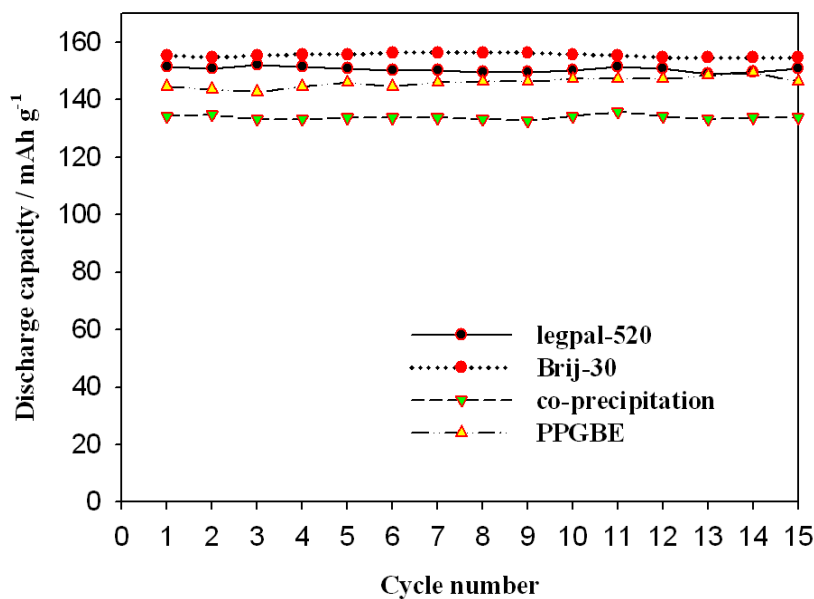


**Figure 7.** AC impedance spectroscopy for  $\text{LiFePO}_4/\text{C}$  prepared with various surfactants.

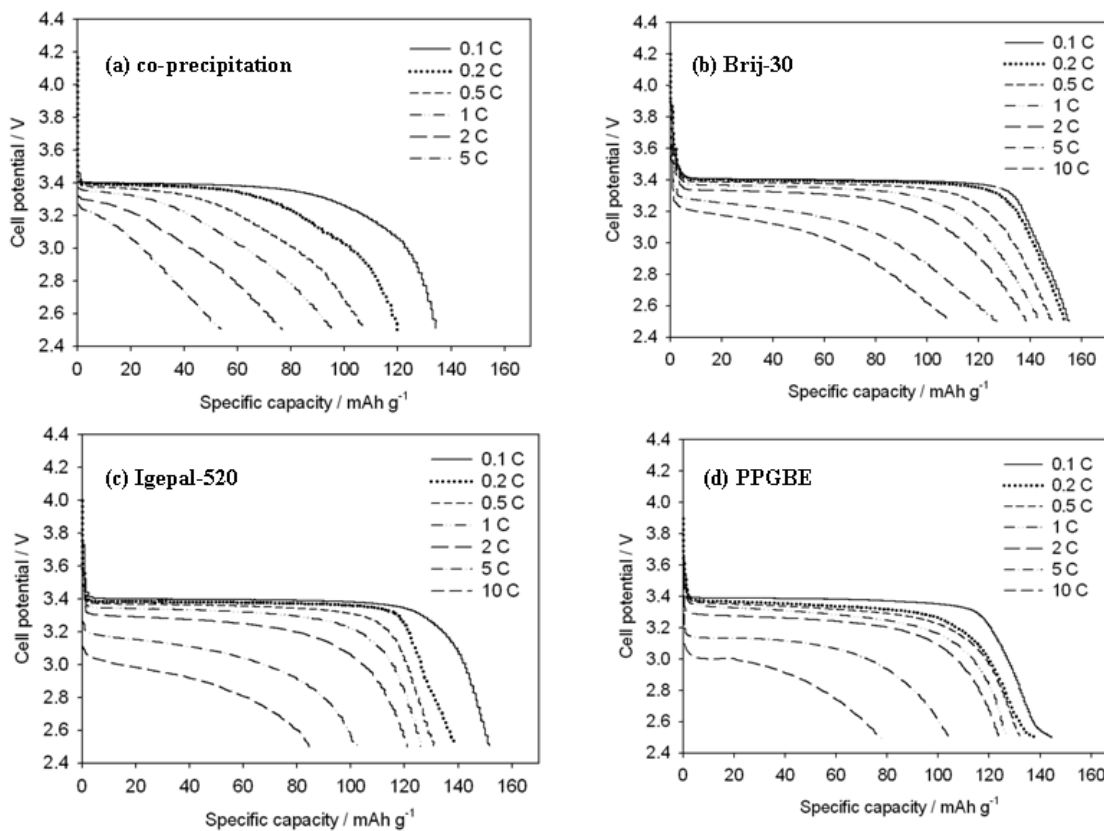
The semicircular plot in the medium frequency range is attributable to the charge transfer resistance ( $R_{ct}$ ) of the electrochemical reaction and the sloping line in the low frequency region represents the diffusion of lithium ions into the bulk of the cathode material, namely the Warburg impedance [25]. In general, a smaller diameter semicircle reflected lower charge transfer resistance and steeper slope reflects lower  $\text{Li}^+$  diffusion impedance. As indicated in Fig.7, the  $R_{ct}$  values for co-precipitation, Brij-30, PPGBE and Igepal-520 are 142, 31, 64 and 62  $\Omega$ , respectively. It is seen that the  $\text{LiFePO}_4/\text{C}$  composites prepared by the emulsion-precipitation route were smaller charge-transfer resistance and larger Li ion diffusion coefficient than that from the co-precipitation method. Generally, the decrease in the resistance to charge-transfer indicates that Li ion and electron transfer are more feasible at the electrode, which is beneficial to the kinetic behavior during charge-discharge process, thereby producing an improvement in electrochemical performance. Furthermore, the Brij-30 exhibits the smallest charge-transfer resistance of the four samples. Therefore, it is expected that the Brij-30 should have excellent kinetic behavior, which is consistent with the CV measurement shown in Fig.6. Also, as shown in Fig.7, the  $\text{Li}^+$  diffusion impedance of PPGBE was lower than Igepal-520 because the particle size was smaller.

Figure 8 shows a plot of discharge capacity versus cycle number for  $\text{Li}/\text{LiFePO}_4$  cells from different samples. All of the cells display stable cycle performance over 15 consecutive cycles.

Obviously, the samples prepared by the emulsion-precipitation exhibits better electrochemical performance.



**Figure 8.** Discharge capacities vs. cycle number at 0.1C rate between 2.5 and 4.2 V for LiFePO<sub>4</sub>/C prepared with various surfactants.



**Figure 9.** Discharge curves of LiFePO<sub>4</sub>/C prepared with various surfactants at variable C-rate.

This is completely consistent with the results from CV and EIS. The cell discharge capacity depends on the types of surfactants. The Brij-30 outperforms all of the other samples because it has a larger intrinsic conductivity and confers the sample with lesser resistance to charge-transfer and better kinetic behavior. Figure 9 shows that discharge curves of LiFePO<sub>4</sub>/C prepared with various surfactants at variable C-rate. It can be seen that all of the samples display similar discharge curves with a potential plateau over a wide voltage range at approximately 3.4 V (vs. Li/Li<sup>+</sup>) at 0.1 C rate. This implies that a two-phase Fe<sup>3+</sup>/Fe<sup>2+</sup> redox reaction proceeds via a first-order transition between FePO<sub>4</sub> and LiFePO<sub>4</sub>. The plateau of the co-precipitation sample disappeared at 0.5C-rate. However, the plateau could maintain the half of the discharge capacity at 2 C-rate for the samples from emulsion-precipitation method.

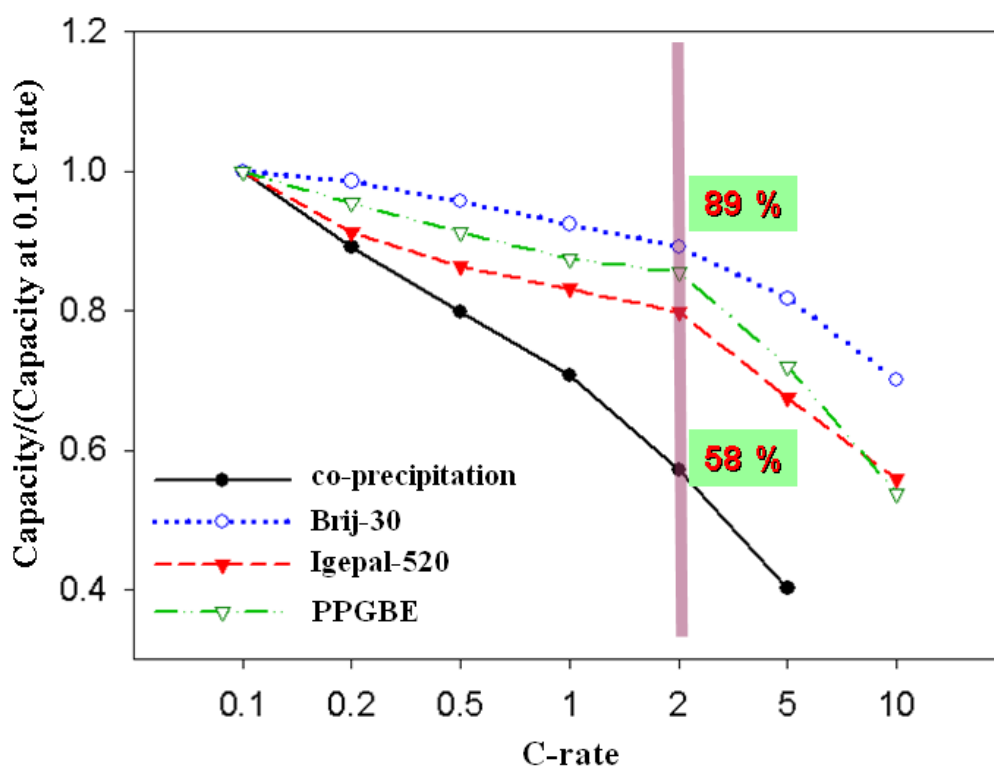


**Figure 10.** Relative specific capacity of LiFePO<sub>4</sub>/C with various surfactants at variable C-rate.

Figure 10 shows relative specific capacity of LiFePO<sub>4</sub>/C with various surfactants at variable C-rate. The cells with surfactants deliver higher at fast discharge rate of 2C. The samples show good capacity for reversal of the cycle with little diminution of capacity at each current density. However, discharge capacity decreases as the discharge rate is increased, which indicates that rate limitations remain. At a rate of 2C, a reversible discharge capacity of approximately 89%, 87%, 80% and 58% of the initial capacity is achieved at a 0.1C rate, for Brij-30, PPGBE, Igepal-520, PPBGE and co-precipitation, respectively. The rate of this decrease is less for the Brij-30 than for the other samples, which is attributable to its larger intrinsic conductivity causing a lesser resistance in the cell.

#### 4. CONCLUSION

Well micro-crystalline LiFePO<sub>4</sub>/C composite powders were prepared using the precipitation method between two reverse-emulsion solutions and investigated using XRD, SEM, TEM, PSA, EA, BET, CV, EIS and charge-discharge tests. The surfactants on the surface of the particles and carbon were uniformly coated on the particle surface after calcination. The micro-sized LiFePO<sub>4</sub>/C composites from emulsion-precipitation method exhibited better electrochemical performance than those composites obtained by classical co-precipitation methods and this is attributable to a greater electronic conductivity and larger coefficient for the diffusion of the Li<sup>+</sup> ion.

The cell discharge capacity and rate capacity depends on the types of surfactants. CV and EIS examination confirmed these results. The highest reactivity and best reversibility at fast rate for Brij-30 because it has a larger intrinsic conductivity and confers the sample with lesser resistance to charge-transfer and better kinetic behavior.

#### ACKNOWLEDGMENT

This authors thank the National Science Council of Taiwan for the financial support in this work under contract no. NSC-98-2113-M-390-002-MY2.

#### References

1. A.K. Padhi, K.S. Nanjundaswamy, and J.B. Goodenough, *J. Electrochem. Soc.* 144, (1997) 1188 - 1194.
2. S.-Y. Chung, J.T. Bloking, and Y.-M. Chiang, *Nat. Mater.* 2 (2002) 123.
3. K. Striebel, J. Shim, V. Srinivasan, and J. Newman, *J. Electrochem. Soc.* 152 (2005) A664.
4. G. Arnold, J. Garche, R. Hemmer, S. Strobele, C. Vogler, and M. Wohlfahrt-Mehrens, *J. Power Sources* 247 (2003) 119-121.
5. H. Huang, S.-C. Yin, and L.F. Nazar, *Electrochem. Solid State Lett.* 4 (2001) A170.
6. Z. Chen and J.R. Dahn, *J. Electrochem. Soc.* 149 (2002) A1184.
7. A. Yamada, S.-C. Chung, and K. Hinokuma, *J. Electrochem. Soc.* 148 (2001) A224.
8. F. Croce, A.D. Epifanio, J. Hassoun, A. Deptula, T. Olczac, and B. Scrosati, *Electrochem. Solid-Sate Lett.* 5 (2002) 47.
9. K.S. Park, J.T. Son, H.T. Chung, S.J. Kim, C.H. Lee, K.T. Kang, H.G. Kim, *Solid State Commun.* 129 (2004) 31.
10. S.Y. Chung, J.T. Bloking and Y.M. Chiang, *Nat. Mater.* 2 (2002) 123.
11. P.S. Herie, B. Ellis, N. Coombs, and L.F. Nazar, *Nat. Mater.* 3 (2004) 147.
12. M. Doeff, Y.Hu, F. McLarnon, and R. Kostecki, *Electrochem. Solid State Lett.* 6 (2003) A207.
13. Y. Hu, M. Doeff, R. Kostecki, and R. Finones, *J. Electrochem. Soc.* 151 (2004) A1279-1285.
14. T. Nakamura, Y. Miwa, M.Tabuchi, and Y. Yamada, *J. Electrochem. Soc.* 153 (2006) A1108.
15. D.R. Sangeeta, X. Zhengkui, and A.P. David, *J. Am. Ceram. Soc.* 73 (1990), 2760-2763.
16. L. Gao, H.C. Qiao, and D.S. Yan, *J. Eur. Ceram. Soc.* 16 (1996) 437-440.
17. M.H. Lee, C.Y. Tai, and C.H. Lu, *J. Eur. Ceram. Soc.* 19 (1999) 2593-2603.
18. L.M. Prince, "Microemulsion Theory and Practice", Academic Press, New York, 1977, p.38.
19. Chi-Wi Ong, Yuan-Kai Lin, and Jenn-Shing Chen, *J. Electrochem. Soc.* 154(6) (2007) A527-A533.
20. H.C. Wong, J.R. Carey, and J.S. Chen, *Int. J. Electrochem. Sci.* 5 (2010) 968-980.
21. Y.H. Nien, J.R. Carey, and J.S. Chen, *J. Power Sources* 193 (2009) 822-827.
22. J.H. Lin and J.S. Chen, *Electrochim. Acta* 62 (2012) 461-467.

23. W.J. Zhang, *J. Power Sources* 196 (2011) 2962-2970.
24. J. Hassoun, K.S. Lee, Y.K. Sun, and B. Scrosati, *J. Am. Chem. Soc.*, 133 (2010) 3139-3143.
25. Ya-Wen Chen and Jenn-Shing Chen, *Int. J. Electrochem. Sci.* 7 (2012) 8128-8139.